Evaluation of Adsorption Parameters and Heats of Adsorption through Desorption Measurements

Bidyut B. Saha,[†] Shigeru Koyama,[†] Ibrahim I. El-Sharkawy,[†,||] Khairul Habib,[†] Kandadai Srinivasan,*[,†,‡] and Pradip Dutta[§]

Interdisciplinary Graduate School of Engineering Sciences, Kyushu University, Kasuga-koen 6-1, Kasuga-shi, Fukuoka 816-8580, Japan, School of Engineering and Logistics, Charles Darwin University, Darwin NT, Australia, and Department of Mechanical Engineering, Indian Institute of Science, Bangalore 560 012, India

The construction of an apparatus for the rapid measurement of the adsorption equilibrium characteristics and evaluation of the isosteric heat of adsorption of activated carbons for gaseous adsorbates is described. The method is based on measuring the amount desorbed between two equilibrium adsorption states. The measurement system has been tested for methane adsorption over (5 to 75) °C and pressures from (2 to 24) bar on a Maxsorb−III specimen of activated carbon. The results are evaluated through regressions with various isotherm equations used in the literature for physisorption and are compared with results of other researchers for comparable adsorbent−adsorbate combinations. A method of accounting for the adsorbed phase volume is proposed.

Introduction

Conclusive evidence emerging on man-made causes of global warming is impelling numerous efforts in various countries for abating greenhouse gas emissions. Adoption of natural gas as the dominant fossil fuel is being promoted widely in several countries. A substantial reduction of carbon dioxide emissions and clean combustion are principal merits of natural gas, whose main ingredient is methane. Compressed natural gas (CNG) is already being used in the transport sector. Intercontinental transport of natural gas is predominantly done through liquefied natural gas (LNG). High pressures of CNG and low temperatures of LNG are impediments in its acceptance in developing countries and in rural/remote settlements of even developed countries. Adsorbed natural gas (ANG) is an intermediary option to CNG and LNG by way of reduction in pressures and near atmospheric temperature storage, albeit through some sacrifice in storage capacity.[1,2] On the other hand, adsorbed storage of methane can also be useful in its controlled release for a fuel cell, when capacity control is required. For these reasons, studies on adsorption of methane on highly microporous solids are desirable, and the topic has drawn the attention of numerous researchers.[3−11] The primary requisites of a prospective specimen of adsorbent for methane storage are high micropore volume and adsorption surface area. Activated carbons with surface areas > 3000 $m^2 \cdot g^{-1}$ and micropore volumes > 1.5 $cm^3 \cdot g^{-1}$ are now commercially available, which are taking ANG closer to viability. The Maxsorb specimens are in this category, and their production methods to achieve the requisite properties are well documented.[12] Methane storage on activated carbons produced from the rice husk base was recently explored.[13] Several investigations on adsorption of methane on these new generation activated carbons are reported in the literature.[14−19]

In general, the adsorption characteristics are obtained through equilibrium volumetric methods[13,14,16−18] or gravimetric methods[3,20] or using a magnetic suspension balance[5,7,8] or chromatographic method.[9] Such measurements must precede the debate on whether or not a particular specimen is amenable for ANG application. However, most of these methods are expensive or time-consuming and can at best give the adsorption and in some cases limited kinetics data. Seldom, the isosteric heat of adsorption is directly measured. Normally one derives them using the isotherm and Clausius−Clapeyron equation. Prakash et al.[21] described a method of evaluating adsorption characteristics of nitrogen on various activated carbons using the desorption method. While it enables a quick estimation of adsorption isotherms, they assess that the method underpredicts the equilibrium concentration. Perhaps, that could be due to limited experimental data and not accounting for structural heterogeniety of pore distribution. In this paper, we describe an improved desorption apparatus for rapid evaluation of adsorption characteristics at relatively low cost and also a method of reducing the errors in data reduction. The apparatus also enables direct assessment of isosteric heats of adsorption. This paper will emphasize both the evaluation of isotherms and isosteric heats of adsorption. The data are fitted to several popular isotherms for physisorption, and it is observed that the new proposed weighting factor correction for adsorbed phase volume gives fairly accurate results.

Materials and Methods

Activated Carbon and the Methane. The Maxsorb specimen labeled as MSC-30 was supplied by Kansai Coke Company (Batch No. 03-07061) with a stated surface area of 3140 $m^2 \cdot g^{-1}$ and a micropore volume (v_μ) of 1.7 $cm^3 \cdot g^{-1}$. It has a mean particle diameter of 72 μm, an ash content of no more than 0.1 %, and moisture of no more than 0.8 %. Its pH is 4.1. The pore size distribution obtained through the nonlocal density functional theory (NLDFT) method is shown in Figure 1. A peak at 2 nm confirms the highly microporous nature of the specimen experimented. The SEM picture at 300 000 magnification is

* Corresponding author. Fax: +61 3 9584 5624. E-mail: mecks@hotmail.com. Currently at Frigrite Refrigeration Pty. Ltd., 27 Grange Road, Cheltenham Vic 3192, Australia.
[†] Kyushu University.
[‡] Charles Darwin University.
[§] Indian Institute of Science.
[||] Mechanical Power Engineering Department, Faculty of Engineering, Mansoura University, El-Mansoura, Egypt.

10.1021/je700369j CCC: $37.00
Published on Web 10/16/2007

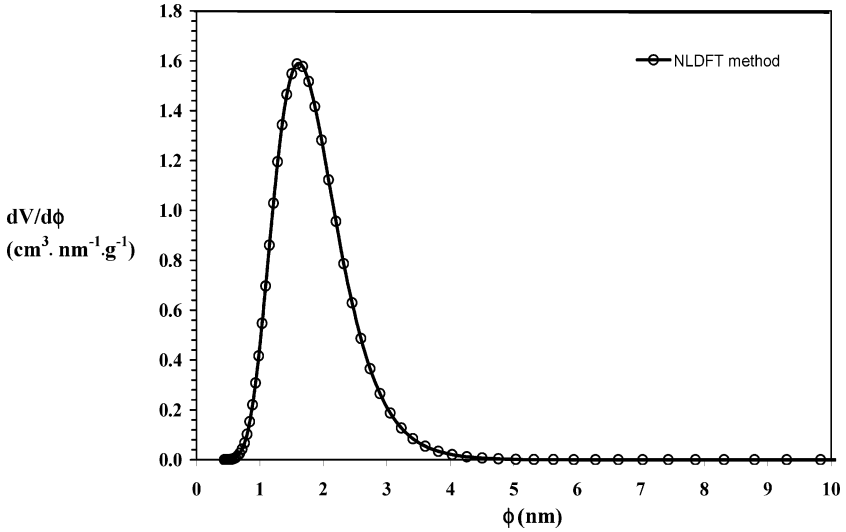

Figure 1. Pore size distribution of Maxsorb−III for the NLDFT method. ϕ indicates the pore width, and $dV/d\phi$ is the incremental pore volume.

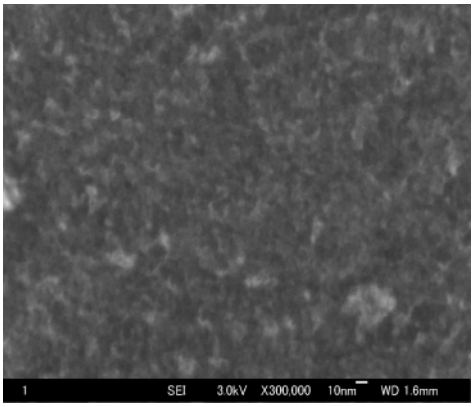

Figure 2. SEM picture of the activated carbon specimen (300 000 magnification).

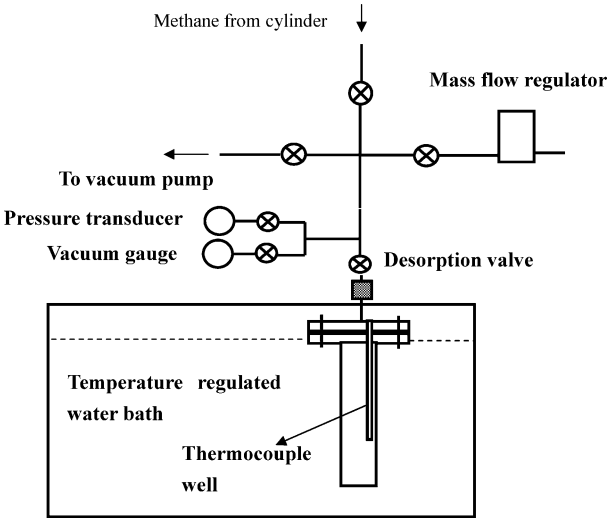

Figure 3. Schematic arrangement of the experimental system.

shown Figure 2. The sample of methane used is 99.999 % pure with the supplier stated impurity levels as follows: N_2 < 5 ppm, CO < 1 ppm, C_2H_6 < 1 ppm, O_2 < 1 ppm, and CO_2 < 1 ppm.

Experimental Apparatus. The experimental apparatus is shown in Figure 3. The adsorption cell is a slender cylindrical unit of internal dimensions of 30 mm diameter and 300 mm depth, giving an enclosed volume (V_{cell}) of ~212 cm^3. It has been designed to withstand pressures to 50 bar even at 150 °C. It was packed with 65.66 g of the activated carbon (m_{ch}) specimen mentioned above, giving a net packing density of 0.31 $g \cdot cm^{-3}$. The external plumbing is made up of 1/4" nominal stainless steel tubes with an internal diameter of 4.35 mm and a set of Swagelok fittings (valves, T's, and crosses). The total internal plumbline volume is estimated to be 13.1 cm^3. A 2 μm filter that is capable of stopping migration of activated carbon particles during evacuation and desorption was fitted in the plumbline at the exit of the cell. A salient feature of the unit is that the cell internal temperature can be measured directly. This is achieved through a thermowell consisting of a fine capillary suspended from the top flange and nipped at the cell end. A thermocouple is inserted in the well for temperature measurement. All metallic materials are made of SS 304.

Instrumentation. The instrumentation consists of (i) a 10 standard liters per minute (at 20 °C and 1.013 bar) mass flow regulator (Kojima- Kofloc-5100) that has a measurement uncertainty of 1 % of full scale (1.67 $cm^3 \cdot s^{-1}$), (ii) a Kyowa-PGS-50KA 50 bar pressure transducer with an uncertainty in measurement of 0.1 % of full scale, (iii) a series of type K thermocouples (supplied by Chino Corp., Japan, uncertainty of 0.6 °C traceable to Japan Calibration Service System standards) precalibrated against a platinum resistance thermometer in a precision temperature bath for measuring temperatures of the cell, the thermostatic bath in which the entire cell is immersed, the ambient, and (iv) a Keithtly 2700 data acquisition system connected to a computer. Data were logged at about 1 s intervals over the entire duration of each process, namely, adsorption, isosteric heating, desorption, and isosteric cooling. The circulating water bath could give a stability of 0.1 °C.

Experimental Procedures. After filling the cell with the activated carbon specimen, it was evacuated down to 25 Pa (measured near the cell) over several days to remove all preadsorbed gases while the cell was baked at about 75 °C in the water bath. The cell was flushed with methane and evacuated first at heated conditions. Then, at the cooled condition of 5 °C, methane was allowed to be adsorbed and then evacuated again while the cell temeprature was raised from (5 to 75) °C. This process of flushing and evacuation was done a few times to ensure that any residual gas was only methane.

Two types of experiments were conducted. In the first, the cell is filled slowly with methane at a temperature of (5 to 10) °C (T_{ads}). After the cell has stabilized (at state 1 in Figure 4), it is isolated and then slowly heated (over several hours) to the

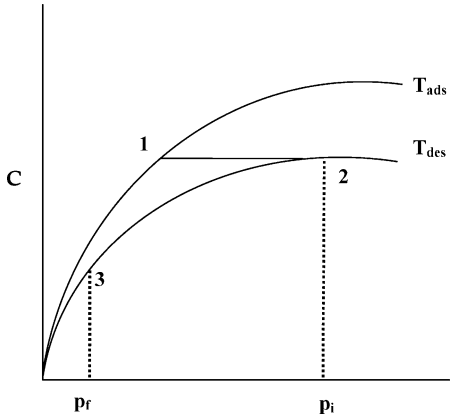

Figure 4. Schematic explanation of experimental sequences.

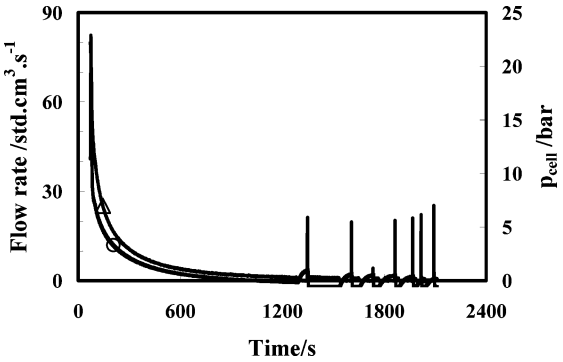

Figure 5. Typical flow and pressure profiles during the slow desorption process. ○, pressure (right ordinate); Δ, flow (left ordinate).

desired temperature of the isotherm. This quasisteady heating process can be construed to be isosteric. The data of the temperature increase with pressure (process 1 to 2) are logged using which isosteric heat of adsorption can be obtained. When the cell reaches equilibrium at the set point of the isotherm (state 2, T_{des}), its pressure at that state is taken as the pressure on the isotherm before desorption (p_i). The cell is gradually desorbed by opening the desorption valve above the cell partially and then the valve upstream of the mass flow regulator. The desorption is allowed over periods of the order of several 100's of seconds. When the flow rate falls to a value that is one order of magnitude higher than the uncertainty, both the valves are closed. This allows the pressure inside the cell to build up again. When it has stabilized, another bout is released. This is repeated several times to get as much gas out as possible. Figure 5 shows typical flow and pressure profiles during a desorption process. The spikes seen in the flow profile are due to bouts of gas being released. When the flow is no longer measurable accurately, the process is stopped. The pressure of the cell is allowed to stabilize, which gives the final pressure after desorption on the isotherm (p_f). A typical pressure recovery profile is shown in Figure 6. In this figure, the temperature recovery profile is also shown. The cell is then allowed to cool if it is at a temperature higher than the ambient or to warm up if it is below, during which the pressure and temperature data are recorded to enable extraction of isosteric heat of adsorption for low uptakes.

In the second method, the methane is adsorbed at a given temperature (state 2) and after stabilization desorbed at the same temperature (2 to 3). In this case, only the isosteric heats of adsorption at low uptakes (after desorption) could be measured.

The experiments were carried out by different groups and in two laps separated by a year. This enabled assessment of the reproducibility of measurements and removing most systematic

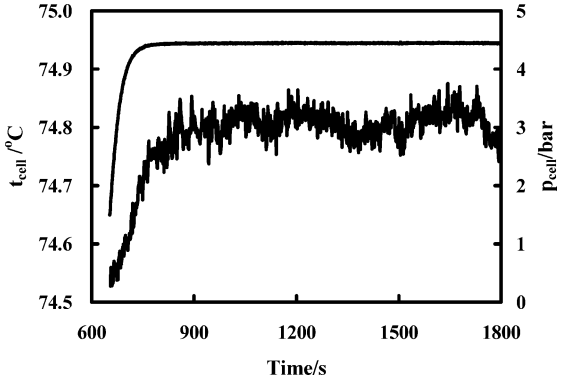

Figure 6. Typical pressure and temperature recovery profiles after desorption. Lines with noise, temperature (left ordinate).

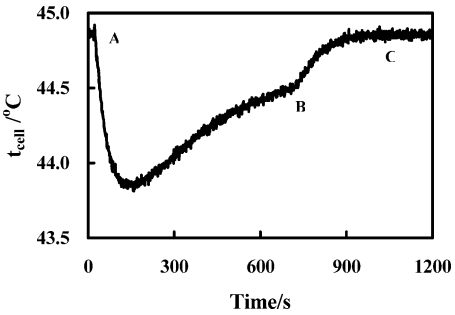

Figure 7. Typical temperature profile of the cell during desorption. A, commencement of desorption; B, end of desorption; B to C, cell temperature recovery after isolation.

Table 1. Raw Data of All Experiments

T_{des}	T_a	p_i	p_f		Δm_{void}	Δm_{pipe}	ΔC
°C	°C	bar	bar	Std L_{des}	g	g	g·g^{-1}
74.8	10.1	24.09	2.24	9.24	0.88	0.18	0.0777
69.8	16.1	18.73	2.83	7.43	0.64	0.13	0.0636
69.8	16.3	21.71	3.00	8.54	0.76	0.16	0.0727
64.5	12.2	22.50	2.96	8.98	0.81	0.17	0.0763
59.8	16.0	14.61	5.45	4.66	0.38	0.08	0.0403
57.7	16.0	12.71	2.97	5.27	0.41	0.08	0.0460
50.0	14.0	13.16	3.40	5.52	0.42	0.08	0.0483
5.0	11.5	10.02	2.69	6.63	0.37	0.07	0.0607
74.4	12.4	11.55	4.45	3.28	0.28	0.06	0.0281
64.5	18.4	11.37	4.55	3.49	0.28	0.06	0.0304
54.5	14.3	11.31	4.24	3.90	0.30	0.06	0.0341
44.4	14.0	11.73	4.92	3.89	0.30	0.06	0.0340
34.5	17.5	11.18	4.30	4.39	0.31	0.06	0.0389
24.3	17.3	11.07	5.36	4.09	0.27	0.05	0.0367
14.4	13.2	11.73	4.70	5.12	0.34	0.06	0.0457
9.3	12.2	11.55	5.29	4.62	0.31	0.06	0.0413

errors associated with the technique of measurement. Table 1 gives the raw data.

Data Reduction

The primary data are the time-dependent flow rate through the mass flow regulator, the cell pressure (p), and cell and ambient temperatures (T_{cell} and T_a). Figure 7 shows the cell temperature during desorption. The temperature of desorption (T_{des}) is deemed to be the integrated average of recorded temperatures between A and B which is the zone over which desorption actually occurs. The flow data are directly reduced to standard liters desorbed (Std L_{des}) by numerical integration of the flow record and converted to total mass desorbed using standard conditions specified by the flow meter manufacturer. This desorbed mass needs to be corrected for the void volume in the cell.[21] The void is divided into two categories, namely, internal cell void and the pipeline volume. It is generally

assumed that adsorption occurs in the micropores, and the void volume (V_{void}) is calculated as follows

$$V_{void} = V_{cell} - \frac{m_{ch}}{\rho_s} - v_\mu m_{ch} \quad (1)$$

Because 65.66 g of cabon has been packed into the cell of 211.95 cm^3, assuming a solid carbon density (ρ_s) of 2.2 $g \cdot cm^{-3}$, the cell void is 70.5 cm^3. The desorbed mass corrections are defined as follows

$$\Delta m_{void} = V_{void}[\rho_i (p_i, T_{des}) - \rho_f(p_f, T_{des})] \quad (2)$$

$$\Delta m_{pipe} = V_{pipe}[\rho_i(p_i, (T_{des} + T_a)/2) - \rho_f(p_f, (T_{des} + T_a)/2)] \quad (3)$$

where ρ is the density of methane and subscripts i and f refer to initial and final states. Because the plumbline volume is only about 6 % of the cell volume, its effect is rather marginal. The density data for methane are taken from web-based calculations (http://webbook.nist.gov/chemistry/fluid).

The main isotherm equations to which the data are regressed are the Langmuir, Toth (as proposed by Himeno et al.),[16] and Dubinin−Astakhov (DA) equations in the following form

$$\frac{C}{C_o} = \frac{k_0 e^{\Delta h_{st}/RT} p}{1 + k_0 e^{\Delta h_{st}/RT} p} \quad (4)$$

$$\frac{C}{C_o} = \frac{p}{\left[\frac{k_0\sqrt{MT}}{e^{\Delta h_{st}/RT}} + p^t\right]^{1/t}} \quad (5)$$

$$W = W_o e^{-[(RT/E)\ln(p_s/p)]^n} \quad (6)$$

where C is the mass concentration ($g \cdot g^{-1}$); $W = Cv_a$; v_a is the adsorbed phase specific volume; R is the universal gas constant (8.314 $J \cdot mol^{-1} \cdot K^{-1}$); and M is the molecular weight of the adsorbate (16.04 for methane). In the case of the DA eq 6, three variations are investigated: namely,

(i) with no adsorbed volume correction whereby eq 6 reduces to

$$C = C_o e^{-[(RT/E)\ln(p_s/p)]^n} \quad (7)$$

and with adsorbed phase volume correction[22]

$$v_a = v_b \exp[\alpha(T_{des} - T_b)] \quad (8)$$

(ii) assigning $\alpha = 0.0025$ as done by Himeno et al.[16] and Amankwah and Schwarz et al.[23] where the subscript b refers to the normal boiling point in the liquid state, and

(iii) allowing a temperature dependence of α such as

$$\alpha = 1/T \quad (9)$$

because α is supposed to represent the isosteric coefficient of the expansion of the adsorbed volume.

The isotherm equations get transformed to the following for desorption at a given temperature between pressures p_i and p_f

$$\Delta C_{T_{des}} = C_o\left[\frac{k_0 e^{\Delta h_{st}/RT_{des}} p_i}{1 + k_0 e^{\Delta h_{st}/RT_{des}} p_i} - \frac{k_0 e^{\Delta h_{st}/RT_{des}} p_f}{1 + k_0 e^{\Delta h_{st}/RT_{des}} p_f}\right] \quad (10)$$

$$\Delta C_{T_{des}} = C_o\frac{p_i}{\left(\frac{k_0\sqrt{MT_{des}}}{e^{\Delta h_{st}/RT_{des}}} + p_i^t\right)^{1/t}} - \frac{p_f}{\left(\frac{k_0\sqrt{MT_{des}}}{e^{\Delta h_{st}/RT_{des}}} + p_f^t\right)^{1/t}} \quad (11)$$

$$\Delta C_{T_{des}} = W_o\frac{e^{-[(RT_{des}/E)\ln(p_s/p_i)]^n} - e^{-[(RT_{des}/E)\ln(p_s/p_f)]^n}}{v_a} \quad (12)$$

Because methane is in the supercritical state in the range of our experiments, the pseudo-saturation pressure p_s at a given desorption temperature is calculated as follows[24]

$$p_s = (T_{des}/T_c)^2 p_c \quad (13)$$

where the subscript c refers to the critical point.

A regression analysis is made to secure the least-squares for deviations between experimental differential concentrations and the RHSs of each of eqs 10 to 12 with variations in the case of eq 12 as per eqs 7 to 9. To evaluate the RHS of eq 10, an initial guess has to be made of isosteric heat of adsorption, which is derivable from our pressure and temperature data logged during heating/cooling. A range of values of k_o and Δh_{st} are used to obtain the least-squares fit. Similarly, in the case of the Toth equation, the parameters to be optimized are t, k_o, and Δh_{st}. In the case of eq 12, the optimized parameters are E and n. In each of these cases, the slope is obtained (C_0 or W_0) for the least sum of squares of differences between the calculated and experimental ΔC's. The entire calculation scheme has been programmed on a spreadsheet.

Assessment of Overall Uncertainty. In addition to uncertainties associated with the instrumentation, averaging the cell temperature during desorption, and the void correction, there will be certain errors introduced due to mathematical regression resulting in deviations between the measured desorption and that obtained from respective equations. It is expected that the overall uncertainty will be within ± 4 % with a minimum of 0.0012 $g \cdot g^{-1}$. In the case of isosteric heat of adsorption, the contributing factors are only the uncertainties in temperature and pressure measurements and the regression (coefficient of regression > 99.9 %); hence, its estimated uncertainty at a given concentration is about 0.5 %.

Results and Discussion

Figure 8 shows a plot of differences on the right-hand sides of eq 12 against ΔW in conjunction with eqs 8 and 9 for the condition of least-squares. The optimized values of W_o and E are listed in Table 2. The intercept is also an indicator of goodness of the fit, which should be 0 in the ideal case. Similarly, Figure 9 shows analogous plots for the cases of eqs 4, 5, and 7. The parameters of the isotherm are listed in Table 3.

Figure 10 makes a comparison of all the isotherm equations, wherein the deviations between experimental and calculated differences between fits are compared. It is seen that the isotherms with $\alpha = 1/T$ are associated with the smallest errors in the group (Tables 2 and 3).

The best way to assess the results is to plot one isotherm wherein all the methods are depicted. This is done in Figure 11. It is seen that Langmuir, Toth, and the proposed volume correction with $\alpha = 1/T$ virtually give identical results. If we were to use $\alpha = 0.0025$, the results would be closer to the experimental results of Himeno et al.[15,16] at 298 K for another specimen of Maxsorb with almost comparable physical characteristics of surface area and micropore volume. From the deviation observed in the case of eq 7, it emerges that the temperature dependence of the adsorbed phase volume cannot be neglected, which could be one of the reasons for underprediction of desorption by Prakash et al.[21] With no temperature

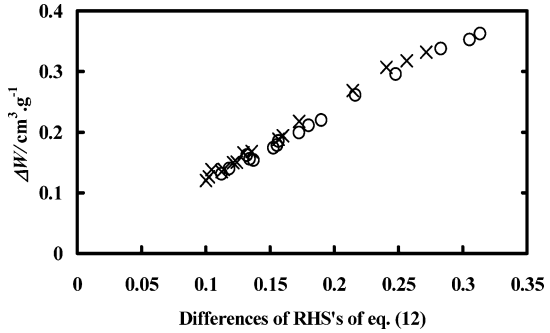

Figure 8. Differences in RHS's of eq 12 vs ΔW. ×, $\alpha = 0.0025$; ○, $\alpha = 1/T$.

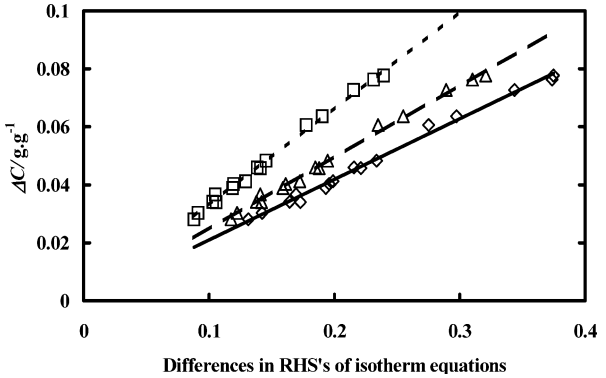

Figure 9. Differences in RHS's of eqs 10 to 12 vs ΔC. ◇, eq 7; Δ, Toth; □, Langmuir.

Table 2. Values of Adsorption Parameters for the Case of Least-Squares

	$\alpha/K^{-1} = 0.0025$	$1/T$
E/J·mol^{-1}	5004	5130
n	1.1	1.42
slope W_0/cm^3·g^{-1}	1.25	1.17
intercept	$-1.7\cdot10^{-3}$	$1.6\cdot10^{-4}$
average error of regression (%)	2.9	2.2

Table 3. Adsorption Parameters for Langmuir, Toth, and DA (without Adsorbed Phase Volume Correction) Isotherms

	Langmuir	Toth	DA with no volume correction
C_0/g·g^{-1}	0.332	0.248	0.209
$(\Delta h_{st}/R)$/K	1170	1307	----
k_o	$5.4\cdot10^{-4}$	$3.1\cdot10^{-8}$	----
E/J·mol^{-1}	----	----	5537
n or t	1	1.3	1.8
intercept	−0.0002	$-8\cdot10^{-5}$	$5\cdot10^{-5}$
average error of regression (%)	2.4	2.4	2.8

dependence, $v_a = 5.6$ cm^3·g^{-1}, whereas with $\alpha = 1/T$, 4.3 < v_a/cm^3·g^{-1} < 4.7 and with $\alpha = 0.0025$, 3.6 < v_a/cm^3·g^{-1} < 4.3. The discrepancies observed in Figure 11 for the cases of the DA equation arise due to variance in E and n required to satisfy least-squares criteria for the amount of methane desorbed.

In Figure 12, we compare the experimental isotherm of some Maxsorb specimens at about 300 K. Here our experimental data are extrapolated between (2.4 and 5) MPa with the isotherm where $\alpha = 1/T$. This figure validates the experimental procedures followed.

Isosteric Heats of Adsorption. Figure 13 shows the ln p vs $1/T$ plot for extracting the isosteric heats of adsorption (Δh_{st}). These plots are generated from direct pressure and temperature measurements during cooling/heating. All experimental data yielded straight lines with regression coefficients > 99.9 %. The slopes $[d(\ln p)/d(1/T)]$ yield the value of $-\Delta h_{st}/R$. The concentration dependence of Δh_{st} is shown in Figure 14, wherein the

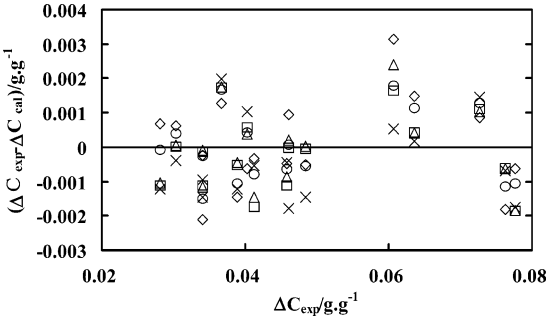

Figure 10. Comparison of deviations between calculated and experimental uptake differences. ×, $\alpha = 0.0025$; ○, $\alpha = 1/T$; ◇, eq 7; Δ, Toth; □, Langmuir.

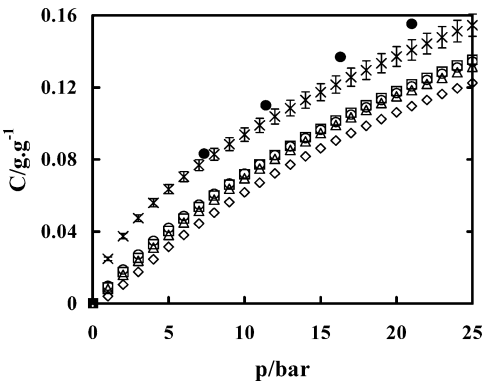

Figure 11. Comparison of all equations considered here for the 298 K isotherm. ×, $\alpha = 0.0025$; ○, $\alpha = 1/T$; ◇, eq 7; Δ, Toth; □, Langmuir; ●, Himeno et al.[16]

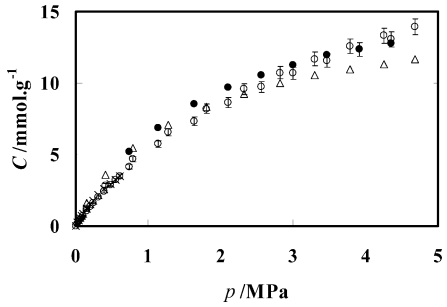

Figure 12. Comparison of isotherm data at about 300 K from various experimental investigations. ●, Himeno et al.[16] at 298 K; ○, present data with eqs 6, 8, and 9 at 298 K; Δ, AX21[19] at 293 K; ×, Maxsorb[14] at 300 K.

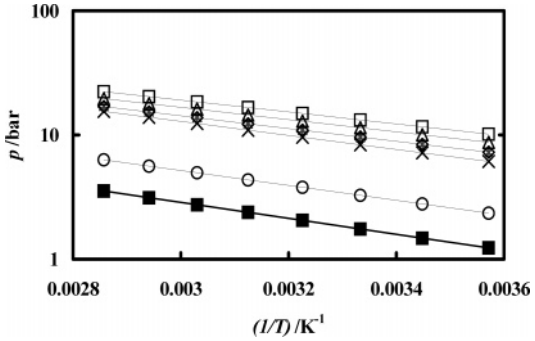

Figure 13. Plot of ln p vs $1/T$ at various concentrations. For C/C_0: ■, 0.059 and 0.086; ○, 0.11; ×, −0.23; ◇, 0.26; Δ, 0.33; □, 0.35.

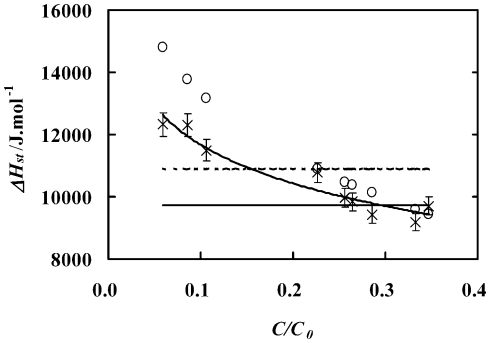

Figure 14. Concentration dependence of isosteric heat of adsorption. ×, experimental values; ○, eq 14; curve, eq 15. Straight lines, lines of Δh_{st} in Langmuir (full line) and Toth (broken line) equation values.

values arrived at using the isotherm equation and the Clausius−Clapeyron equation with $\alpha = 1/T$ are also shown. The latter can be derived from eq 6 as follows

$$\Delta h_{st} = E\left[\left(\ln\frac{W_0}{C\upsilon_a}\right)^{1/n} + \frac{T_b}{nT}\left(\ln\frac{W_0}{C\upsilon_a}\right)^{(1-n)/n}\right] + 2RT \quad (14)$$

Because the temperature varies during isosteric heating/cooling, the harmonic mean temperature of the starting and ending values was taken and υ_a was calculated at this temperature. The best fit for directly extracted data in Figure 14 (×) is correlated as follows

$$\Delta h_{st}\ (\mathrm{J{\cdot}mol^{-1}}) = 7544 + 1793\ln(C_0/C) \quad (15)$$

which reproduces experimental data with a mean error of 3 %, and the error bars are depicted in this figure.

While a fairly good agreement between direct extraction of isosteric heat of adsorption during heating/cooling and the values derived from isotherms is observed at high relative uptakes, the deviations at low relative loadings are quite significant. The optimal values from Langmuir and Toth equations are also shown in the above figure, which are within the limits of experimental values. The Langmuir and Toth equations do not account for the concentration dependence of isosteric heats of adsorption. The differences between the isosteric heats of adsorption between extracted values and those derived from isotherm equations are attributable to temperature and pressure dependence of the adsorbed phase volume, while only temperature dependence has been considered here. This has also been observed by El-Sharkawy et al.[25]

Conclusions

An experimental apparatus for rapid evaluation of adsorption equilibrium characteristics and extraction of isosteric heats of adsorption from temperature and pressure data during heating/cooling has been developed, and its performance is validated through measurement of methane adsorption on Maxsorb−III. The data are regressed to various isotherm equations applicable to this pair. A good match between the present data and those from other sources on comparable pairs is observed. There is a fair agreement even in isosteric heats of adsorption, although the deviations are significant at low loading. The apparatus could be handy for evaluation of suitability of an adsorbent−adsorbate pair a priori, in general, for gas storage and refrigeration applications.

Literature Cited

(1) Barbosa Mota, J. P.; Rodrigues, A. E.; Saatdjian, E.; Tondeur, D. Dynamics of natural gas adsorption storage systems employing activated carbon. *Carbon* **1997**, *35*, 1259−1270.
(2) Basumatary, R.; Dutta, P.; Prasad, M.; Srinivasan, K. Thermal modeling of activated carbon based adsorptive natural gas storage system. *Carbon* **2005**, *43*, 541−549.
(3) Alcañiz-Monge, J.; De La Casa-Lillo, M. A.; Cazorla-Amorós, D.; Linares-Solano, A. Methane storage in activated carbon fibers. *Carbon* **1997**, *35*, 291−297.
(4) Biloé, S.; Goetz, V.; Guillo, A. Optimal design of an activated carbon for an adsorbed natural gas storage system. *Carbon* **2002**, *35*, 1295−1308.
(5) Frère, M. G.; De Weireld, G. F. High-pressure and high-temperature excess adsorption isotherms of N_2, CH_4 and C_3H_8 on activated carbon. *J. Chem. Eng. Data* **2002**, *47*, 823−829.
(6) Malbrunot, P.; Vidal, D.; Vermesse, J.; Chahine, R.; Bose, T. K. Adsorption measurements of argon, neon, krypton, nitrogen, and methane on activated carbon up to 650 MPa. *Langmuir* **1992**, *8*, 577−580.
(7) Bastos-Neto, M.; Torres, A. E. B.; Azevedo, D. C. S.; Cavalcante, C. L., Jr. A theoretical and experimental study of charge and discharge cycles in a storage vessel for adsorbed natural gas. *Adsorption* **2005**, *11*, 147−157.
(8) Herbst, A.; Harting, P. Thermodynamic description of excess isotherms in high-pressure adsorption of methane, argon and nitrogen. *Adsorption* **2002**, *8*, 111−123.
(9) Dreisbach, F.; Staudt, R.; Keller, J. U. High pressure adsorption data of methane, nitrogen, carbon dioxide and their binary and ternary mixtures on activated carbon. *Adsorption* **1999**, *5*, 215−227.
(10) Van der Vaart, R.; Bosch, H.; Cindy, H.; Reith, T. Single and mixed gas adsorption equilibria of carbon dioxide/methane on activated carbon. *Adsorption* **2000**, *6*, 311−323.
(11) Choi, B. K.; Choi, D. K.; Lee, Y. W.; Lee, B. K.; Kim, S. H. Adsorption equilibria of methane, ethane, ethylene, nitrogen and hydrogen onto activated carbon. *J. Chem. Eng. Data* **2003**, *48*, 603−607.
(12) Otowa, T.; Tanibata, R.; Itoh, M. Production and adsorption characteristics of MAXSORB: high-surface-area active carbon. *Gas Sep. Purif.* **1993**, *7*, 241−245.
(13) Balathanigaimani, M. S.; Kang, H. C.; Shim, W. G.; Kim, C.; Lee, J. W.; Moon, H. Preparation of powdered activated carbon from rice husk and its methane adsorption properties. *Korean J. Chem. Eng.* **2006**, *23*, 663−668.
(14) Sheikh, M. A.; Hassan, M. M. I.; Laughlin, K. F. Adsorption equilibria and rate parameters for nitrogen and methane on Maxsorb activated carbon. *Gas Sep. Purif.* **1996**, *10*, 161−168.
(15) Himeno, S.; Komatsu, T.; Fujita, S. Development of a new effective biogas adsorption storage technology. *Adsorption* **2005**, *11*, 899−904.
(16) Himeno, S.; Komatsu, T.; Fujita, S. High pressure adsorption equilibria of methane and carbon dioxide on several activated carbons. *J. Chem. Eng. Data* **2005**, *50*, 369−376.
(17) Zhou, L.; Zhou, Y.; Li, M.; Chen, P.; Wang, Y. Experimental and modeling study of the adsorption of supercritical methane on a high surface activated carbon. *Langmuir* **2000**, *16*, 5955−5659.
(18) Li, M.; Gu, A. Z.; Lu, X. S.; Wang, R. S. Supercritical methane adsorption equilibrium data on activated carbon with prediction by the adsorption potential theory *J. Chem. Eng. Data* **2004**, *49*, 73−76.
(19) Zhou, L.; Ming, L.; Zhou, Y. Measurement and theoretical analysis of the adsorption of supercritical methane on super activated carbon. *Sci. China* **2000**, *43*, 143−153.
(20) Salem, M. M. K.; Braeuer, P.; Szombathely, M. V.; Heuchel, M.; Harting, P.; Quitzsch, K.; Jaroniec, M. Thermodynamics of high-pressure adsorption of argon, nitrogen, and methane on microporous adsorbents. *Langmuir* **1998**, *14*, 3376−3389.
(21) Prakash, M.; Mattern, A.; Prasad, M.; Sant Ram; Subramanya; Srinivasan, K. Adsorption parameters of activated charcoal from desorption studies. *Carbon* **2000**, *38*, 1163−1168.
(22) Ozawa, S.; Kusumi, S.; Ogino, Y. Physical Adsorption of Gases at High Pressure. *J. Colloid Interface Sci.* **1976**, *56*, 83−91.
(23) Amankwah, K. A. G.; Schwarz, J. A modified approach for estimating pseudo-vapor pressure in the application of the Dubinin-Astakhov equation. *Carbon* **1995**, *33*, 1313−1319.
(24) Dubinin, M. M. The potential theory of adsorption of gases and vapors for adsorbents with energetically nonuniform surfaces. *Chem. Rev.* **1960**, *60*, 1−70.
(25) El-Sharkawy, I. I.; Saha, B. B.; Koyama, S.; Srinivasan, K. Isosteric heats of adsorption extracted from experiments of ethanol and HFC 134a on carbon based adsorbents. *Int. J. Heat Mass Transfer* **2007**, *50*, 902−907.

Received for review July 2, 2007. Accepted September 1, 2007. This work was partially supported by the Ministry of Education, Culture, Sports, Science and Technology (MEXT), Japan, "Science and Technology Project", Project No. 18650205.

JE700369J